



1 **Addition of brackish water to tundra soils does not inhibit**
2 **methane production: implications for Arctic coastal methane**
3 **production**

4 **Alexie Roy-Lafontaine**^{1, 5}, Rebecca Lee², Peter M.J. Douglas^{3, 4}, Dustin Whalen², André
5 Pellerin^{1,5}

6 ¹Institut des Sciences de la Mer, Université du Québec à Rimouski, Rimouski, Québec, Canada et Centre de recherche
7 Geotop

8 ²Geological Survey of Canada, Natural Resources Canada, Halifax, Nova Scotia, Canada

9 ³Department of Earth and Planetary Sciences and Geotop Research Centre, McGill University, Montréal, Québec,
10 Canada

11 ⁴Centre d'Études Nordiques, Université Laval, Québec, Québec, Canada

12 ⁵Québec Océan, Université Laval, Québec, Québec, Canada

13 *Correspondence to:* Alexie Roy-Lafontaine (alexieroylafontaine@gmail.com)

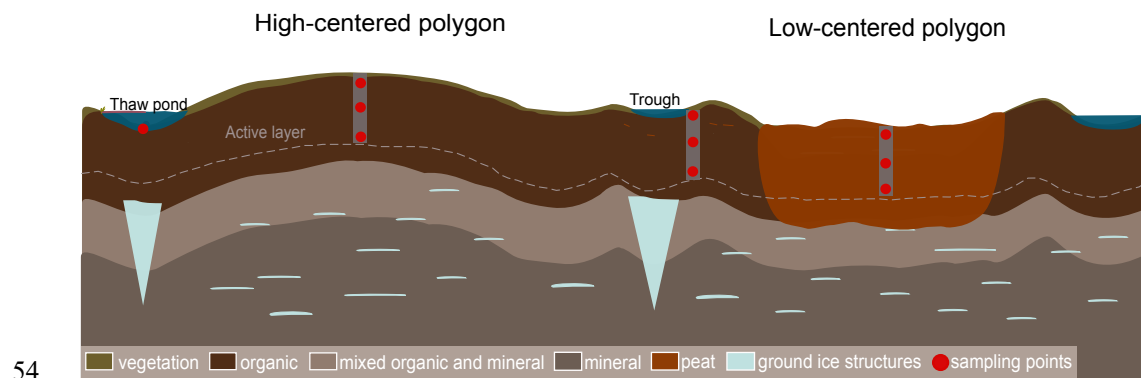
14 **Abstract.** In Arctic regions where coastal sediments contain permafrost, global climate change drives processes such
15 as erosion and subsidence. The contribution of these processes to carbon emissions are still uncertain. Relative sea
16 level rise can lead to more waterlogged environments, promoting anoxic degradation of organic matter but it can also
17 lead to a greater exposure of coastal sediments to seawater. This could alter methane (CH₄) production dynamics,
18 although the controls remain poorly understood. For instance, sulfates contained in seawater may have a tampering
19 effect on methanogenesis through competitive inhibition but the increase in microbial abundance could enhance
20 methanogenesis. In this study, we present CH₄ production rates alongside geochemical analyses in a rapidly evolving
21 coastal landscape near the community of Tuktoyaktuk, NWT, Canada, which is located in the continuous permafrost
22 zone. To better constrain CH₄ production dynamics along the land to ocean continuum, sediment profiles were
23 collected from nearshore marine sediments, as well as from the active layer of the coastal (intertidal) zone and inland
24 soils. Anoxic incubations were performed, amended with brackish water to simulate the effect of seawater on the
25 breakdown of organic matter and the production of CH₄. We found marine sediments expectedly led to negligible
26 CH₄ production rates, while the inland sites showed variable rates between null and 35 nmol cm⁻³ d⁻¹. The coastal
27 (intertidal) zone had the highest rates reaching 415 nmol cm⁻³ d⁻¹. Interestingly, sulfate present in brackish water and
28 sediments did not suppress methanogenesis in the incubations of the coastal and inland zones. Analyses of stable
29 carbon isotopes from CH₄ produced in the incubation experiment indicated greater acetotrophy and higher organic
30 matter lability in the coastal zone, possibly contributing to higher CH₄ production rates. This study highlights the
31 potential for significant CH₄ emissions even with high sulfate concentrations which are classically thought to inhibit
32 methanogenesis. This suggests that Arctic coastal microbial CH₄ production might be an understudied source to the
33 atmosphere.



34 1 Introduction

35 Arctic coastal ecosystems are impacted by sea level rise, coastal erosion, land submersion, higher frequency in storm
36 events and permafrost degradation (AMAP 2019; Guimond et al., 2021; Irrgang et al., 2022; Lantuit et al., 2013; Lim
37 et al., 2020). The amplification of coastal environmental changes has impacts on biogeochemical cycles (AMAP,
38 2017) and on organic matter (OM) degradation processes and fluxes at the land-ocean continuum (Tanski et al., 2021).
39 Furthermore, the progressive thawing of permafrost exposes long frozen organic matter to microbial decomposition
40 (Lapham et al., 2020; Pellerin et al., 2022; Schuur et al., 2015), leading to the release of greenhouse gases like carbon
41 dioxide (CO₂) and methane (CH₄). Inputs and outputs of the Arctic carbon biogeochemical cycle are known to be
42 reshaped by rapid environmental changes (Couture et al., 2018), but processes in coastal settings are still poorly
43 understood.

44 Rates of coastal change vary according to the morphology of coastal landscapes (Manson et al., 2019). The
45 average rate of land retreat measured in the Tuktoyaktuk Coastlands (North-West Territories, Canada), our study site,
46 between 1985 and 2020 was -1.06 m/yr, while processes of ground subsidence and submersion induced retreat rates
47 higher than -4 m/yr (Costa, 2022) which can inundate large swaths of land. Inundated tundra flats and polygons are
48 widespread landforms in the landscape (Costa, 2022). Polygon tundra flats are characterized by ice-wedge polygons,
49 which are formed by the repeated thermal contraction and expansion of the upper layers of the permafrost (Steedman
50 et al., 2016). At the surface, the polygons are expressed as minor topographic features separated by lower-lying, often
51 wet or inundated channels called troughs (Fig 1). Polygons can be classified as low-centered (with a low, wet center
52 and raised rims) or as high-centered (with well-drained centers and lower well-drained rims) (Fig 1), exhibiting strong
53 thermal, hydrological and geochemical gradients (Vaughn et al., 2016).



55 **Figure 1.** Schematic representation of polygonal tundra with peat accumulation as seen in continuous permafrost
56 environments. High-centered polygons are associated with drier conditions, while low-centered polygons, troughs and
57 pondlets are associated with humid or water-saturated conditions. Vegetation cover and OM reflect the hydrology of
58 sites. Not to scale.

59



60 Hydrological conditions in polygons play a pivotal role in shaping the pathways of OM decomposition and
61 consequently influence the resulting CO₂ and CH₄ production. Well drained oxic conditions allow microbes to
62 decompose OM rapidly, leading to the production of CO₂ (Jones et al., 2020). Conversely, water saturation restricts
63 oxygen availability, promoting anaerobic respiration and fermentation, thus inducing both CO₂ and CH₄ production
64 (Lipson et al., 2012; Turetsky et al., 2008). Thus, coastal changes can swiftly alter water saturation conditions in
65 polygons, in many cases significantly enhancing fermentation and CH₄ production (Elberling et al., 2013; Holm et al.,
66 2020; Treat et al., 2015).

67 Furthermore, coastal changes can also influence the chemistry of the water within soils, which can affect OM
68 degradation. In anaerobic conditions, OM degradation processes follow a sequence of electron acceptors of decreasing
69 energetic yields with nitrate, manganese oxides, iron oxides and sulfate as the most abundant electron acceptors
70 (Froelich et al., 1979). It is when all alternative electron acceptors are depleted that fermentation takes place, leading
71 to the production of CH₄; methanogenesis. For example, in beach, estuarine mudflats and marsh mudflats on the
72 Brittany coast (France), OM degradation is dominated by sulfate reduction; the abundance in sulfate from seawater
73 inhibits methanogenesis through competitive inhibition (Winfrey and Ward, 1983). By contrast, OM degradation in
74 sediments below thermokarst lakes, which are anoxic and devoid of alternative electron acceptors, is completely
75 dominated by methanogenesis (Sepulveda-Jauregui et al., 2015). The aqueous chemistry therefore plays a critical role
76 in determining OM degradation. CH₄ produced in soils or sediments can also be oxidized by anaerobic methanotrophic
77 archaea and sulfate-reducing bacteria (Boetius et al., 2000; La et al., 2022) present in the soils or sediment, contributing
78 to lower CH₄ emissions in coastal environments. Thus, on or near the coast, the interaction with seawater, which
79 contains electron acceptors such as sulfate, can shift the OM mineralization pathway and the resulting CO₂ and CH₄
80 productions. Consequently, a nuanced understanding of biogeochemical processes and their drivers is paramount in
81 determining the magnitude of permafrost carbon emissions, especially from coastal environments.

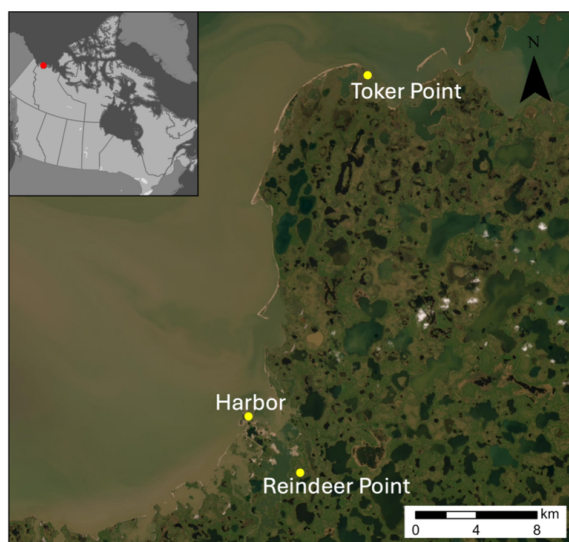
82 Numerous CH₄ emissions monitoring programs are in operation, but remote-sensing methods lack the ability
83 to comprehensively capture the microbial, biogeochemical and environmental processes involved. In specific regions,
84 estimates of methane production from the breakdown of OM is possible by carefully studying degradation pathways
85 and production rates (Pellerin et al., 2022; Heslop et al., 2015; Knoblauch et al., 2018; Treat et al., 2014). To reduce
86 the knowledge gap of CH₄ biogeochemistry in coastal permafrost settings, we collected material from the active layer
87 for incubation experiments, which were coupled to physical and chemical characterizations. The main objective of
88 this study was to assess microbial CH₄ production dynamics in a coastal permafrost setting and apply it at the landscape
89 level, since methane production is well documented in inland thermokarst but is not well understood in a land-ocean
90 interaction context. We hypothesized that methanogenesis in coastal active layer incubations would be suppressed by
91 the addition of sulfate. Consequently, we discuss the influence of environmental conditions on microbial CH₄
92 production with an emphasis on brackish water addition in coastal soils and sediments along with the microbial
93 pathways involved. We then apply these results at the landscape level to provide an estimate of CH₄ production in the
94 event that a natural process like a storm inputs brackish water over a large area of polygonal patterned ground. We
95 use the region around Tuktoyaktuk as an example.



96 **2 Methods**

97 **2.1 Site description and sampling**

98 Tuktoyaktuk (69°26'24'' N, 133°01'52''W) is located in the Inuvik region of the North-West Territories,
99 adjacent to the Arctic Ocean in the Kugmallit Bay, east of the Mackenzie Delta. The region experiences prolonged
100 cold winters, short cool summers, and year-round low precipitation, fostering low-arctic tundra vegetation. Lying in
101 the continuous permafrost zone, its coastal areas feature thick Quaternary and glaciogenic unconsolidated deposits
102 (Rampton, 1988), where permafrost thickness averages 400 m (Hu et al., 2013) and is characterized by prevalent
103 ground ice structures (Mackay and Dallimore, 1992; Martin et al., 2018; Murton, 1996; Rampton, 1988). The area
104 has been ice-free for the past 13 000 years, with evidence indicating that early Holocene summer temperatures were
105 up to 6°C warmer than today, fostering vegetation and peat accumulation (Dallimore et al., 1997; Vardy et al., 1997).
106 During that same period, sea level was considerably lower than it is today and the Tuktoyaktuk area was located
107 approximately 100 km inland (Vardy et al., 1997). Currently, ground subsidence and coastal erosion are major causes
108 of rapid land retreat (Hynes et al., 2014; Lapham et al., 2020; Lim et al., 2020). Combined with sea level rise (Hill et
109 al, 1993), it is projected that a substantial amount of terrestrial soil will become part of the ocean seafloor either by
110 erosion and deposition or by subsidence of land and submersion. Over the past 15 years, extensive studies on
111 Tuktoyaktuk's coastal environment, driven by the region's vulnerability to climate change, highlighted challenges for
112 the Inuvialuit population relying on hunting, fishing, trapping and harvesting (Andrachuk and Smit, 2012).



113

114 **Figure 2.** Map of study area indicating the sampled sites with yellow dots (ESRI, 2022). Harbor site is located in the
115 marine waters, Toker Point site is located in the coastal (intertidal) zone and Reindeer Point site is located inland.

116



117 Active layer samples were collected from three sites: an inland site, Reindeer Point (RP), a coastal site, Toker Point
118 (TP) and a marine site, Harbor. RP was selected as the inland site because it features a polygonal patterned ground
119 typical of the region, and is located in a stable region not directly affected by coastal processes such as storm surges,
120 tides, seawater intrusion, erosion etc. The thermokarst lake margin, about 300m south of RP has remain unchanged
121 since aerial photos began recording the evolution of the landscape in 1947 (Fig S1). TP was selected as the coastal
122 site because of the strong coastal processes such as tides and storm surge that regularly lead to seawater intrusion in
123 this polygonal patterned ground, strongly influenced by ground subsidence. The Harbor site was selected about 400
124 m offshore in the Harbor of Tuktoyaktuk where cold marine bottom waters are overlain at about 10m depth by a
125 surface brackish water layer. The water depth was 20 m. Sediments were collected using a UWITEC gravity corer.
126 The sediments consisted of recently deposited silty sands originating from the strong erosional processes occurring in
127 the region (Whalen et al., 2022). The site was accessible by small watercraft. At RP and TP sites, the soil profiles were
128 extracted from the active layer by digging a soil pit with a shovel. To retain an intact stratigraphic relationship, samples
129 were taken from the wall of the soil pit. Biogenic ebullition gases were collected from pondlets at RP and TP. Pondlets
130 were located within sampled polygonal patterned ground and are defined as small (1 to 3 m²) and shallow standing
131 bodies of water, potentially draining seasonally. Samples were trapped using a plastic funnel attached to a 20 mL glass
132 vial. Surface soil lying at the bottom of the pondlets (Fig. 1) were poked until the vial was filled with gas. Once full,
133 vials were crimped with 20 mm butyl rubber stoppers and aluminum caps. Samples were kept frozen until the time of
134 analyses.

135 The inland site, (RP), was located 750 m from the coast and 2 km East of Tuktoyaktuk in a polygonal
136 patterned ground. This patterned ground is located in a depression, surrounded by elevated plateaus with observable
137 ground water flowing into the valley. In this area, low-centered polygons exhibited higher moisture levels compared
138 to high-centered polygons. High-centered polygons were colonized by shrubs and small flowering plants like
139 *Ericaceae*, while low-centered polygons were dominated by hydrophilic plants such as grasses and sedges. Wet
140 troughs delimited the polygons, with vegetation reflecting waterlogged conditions. The mean active layer thickness
141 across RP was about 35 cm. Profile 10A was collected from a trough and presented water-saturated conditions with
142 brown OM. Profiles 10B and 10D were collected from high-centered polygons and characterized by unsaturated
143 conditions with dark brown OM and presence of roots until 20 cm depth. Profile 10C was collected from a low-
144 centered polygon and consisted of reddish-brown peat throughout. Profiles 10A, 10B and 10D did not consist of peat.

145 The coastal site (TP) is located 20 km NW of Tuktoyaktuk, featuring a polygonal patterned ground, largely
146 colonized by *Carex sp.*, a type of graminoid plant common near Arctic coastlines. The mean active layer depth was 35
147 cm. The site's dynamics are influenced by the twice-daily ebb and flow of tides. Profile 07 was collected from a water-
148 saturated low-centered polygon, located in the intertidal zone. The soil color was very dark greyish black. Profile 08
149 was collected from a water-saturated polygonal trough not immediately located in the intertidal zone, but which floods
150 during storms. The soil was characterized by dark greyish-brown OM mixed with sand. Finally, profile 09, was
151 collected from the center of a higher-centered polygon situated in the middle intertidal zone. The active layer appeared



152 water unsaturated. The soil from this site consisted of a mixture of black organic-rich material and sand. The sand
153 found in samples from TP appeared to be wind-deposited from nearby dunes.

154 **2.2 Sulfates and chlorine concentrations in sediments**

155 The extraction of sulfate and chloride from sediments and soils pore-water was conducted through a leaching
156 experiment following Lacelle (2019). Frozen aliquots of sediments and soils were thawed at 4°C overnight, then
157 weighed, dried in the oven at 60°C for 24 hours and re-weighed to determine the densities. Aliquots of dried material
158 were put in 50 mL falcon tubes with nanopure water following a 1:10 ratio. Tubes were then shaken for one hour to
159 promote leaching of anions towards the aqueous phase of the solution. Once the leaching process was done, 2 mL of
160 the aqueous solution was filtered using 0.2 µm pore size Whatman 25 mm GD/X syringe filters and transferred in
161 disposable microtubes. Concentrations of sulfate and chloride were measured by ion chromatography using a Thermo
162 Dionex Integrion at UQAR's Chemistry department facilities with a limit of detection of 0,01 µg/mL. The measured
163 concentrations are expressed in mmol g⁻¹ wet-weight⁻¹ of material (mmol g⁻¹ wweight⁻¹). Only one measurement per
164 sample was performed as stability tests revealed variability of less than 3% between measured samples. The error on
165 each value was calculated by the least squares method (Skoog et al., 2014).

166 **2.3 Methane production rates in incubations**

167 Long-term sediment and soil incubations under anoxic conditions were used to assess CH₄ production rates
168 over several months by measuring CH₄ accumulation in the vials' headspace. The objective was to simulate the
169 increased connectivity between the land and the ocean in the coastal environment of the Canadian Arctic, which
170 represents an important aspect of the ongoing regional environmental transition. Collected sediments and soil profiles
171 were immediately sub-sampled based on depth, at 5 or 10 cm intervals, according to shifts in sedimentary units. To
172 prepare incubations, about 4 mL of sediment and exactly 2 mL of brackish water (collected from the coast) were
173 immediately transferred into 20 mL glass vials. Incubation vials were crimped with 20 mm blue chlorobutyl rubber
174 stoppers and aluminum caps. The bottles were flushed with nitrogen gas (Alpha Gaz 1) at a rate of 300mL/min for 2
175 minutes in the field to replace the air with a nitrogen atmosphere. Four incubations were prepared for each sampled
176 depth; 3 were kept for measurements of CH₄ production rates (triplicates) and one served for isotopic analyses.
177 Incubations were kept at 4°C and incubated for 339 days in total. The brackish water added to all incubations contained
178 5.7 ± 0.0 mmol g⁻¹ wweight⁻¹ of sulfate and 28.7 ± 0.5 mmol g⁻¹ wweight⁻¹ of chloride.

179 Analyses of the CH₄ concentrations in the headspace of the vials were performed on a gas chromatograph
180 (Agilent 8900) equipped with a flame ionization detector (GC-FID) at UQAR facilities. The GC-FID is equipped with
181 a 100 µL injection loop to ensure a consistent volume of sample is analyzed. To saturate the injection loop, 300 µL
182 are taken from the headspace of the vials and transferred to the injection loop with a gas-tight syringe. Prior to
183 injection, samples were shaken for 30 seconds to equilibrate headspace and sediment gases. This procedure was done
184 every two weeks for 16 weeks to measure CH₄ accumulation in the headspace. The resulting production rates were
185 back calculated, and values are expressed in nmol of CH₄ per cubic centimeters of wet material per day (nmol cm⁻³ d⁻¹)
186 ¹). The density of the collected samples varied widely, with some being organic deposits and peat, while others



187 contained higher mineral content. Consequently, the CH₄ production rates were expressed volumetrically to account
188 for these discrepancies which are more representative of the volume they occupy in the soils profiles and landscape.
189 The limit of detection of the GC-FID is 0.3 ppm and all samples had higher concentrations. Each value represents the
190 mean of triplicate measurements and the reported uncertainty on the measurement is the standard deviation on
191 triplicates.

192 To estimate the potential total active layer CH₄ production (T), the active layer production rates were
193 vertically integrated to obtain the total production of each profile. Values are reported in mmol m⁻² d⁻¹ and were
194 calculated using eq. 1:

$$195 \quad T = \frac{1}{100} \sum_{i=1}^n P_i \cdot e_i \quad [mmol \, m^{-2} \, d^{-1}]$$

196 Where P_i represents CH₄ production rate in layer i (nmol cm⁻³ d⁻¹), e_i represents the thickness of layer i (cm)
197 and n represents the numbers of layers in the profile.

198 Using aerial imagery from 2022, the polygonal tundra at RP was mapped in QGIS, allowing for the
199 discrimination between high-centered polygons, low-centered polygons and throughs (Fig S2). The total area of each
200 geomorphological form was calculated based on the map data (Table S1). Landforms total areas were multiplied by
201 the corresponding potential total active layer methane production (T) to estimate the total CH₄ produced in the
202 polygonal tundra of RP over a day (mol d⁻¹).

203 **2.4 Elemental and isotope composition of the sediment**

204 The total organic carbon (TOC) content of the sediments was measured by combustion using an elemental
205 analyzer (ECS 8020, NC Technologies) combined with a gas chromatograph equipped with a thermal conductivity
206 detector at ULaval facilities (The International Research Laboratory Takuviik). A 100 mg aliquot of sediment was
207 thawed and weighed for each sample. They were then dried in an oven at 60°C for 48 hours and re-weighed to
208 determine their water content. Sediments were then ground using a granite mortar pestle and homogenized using a
209 1.18 mm pore size sieve to remove roots and rootlets. Instruments were cleaned with ethanol between manipulations.
210 Inorganic carbon was removed from sediments by adding 2.2 mL of 12M HCl in every sample. After reacting for 24
211 hours, around 8 mg was encapsulated in tin foil capsules. Samples were kept in a desiccator until analyses. Values are
212 expressed as % of carbon contained in the weighed sample (wt. %).

213 The organic carbon ($\delta^{13}\text{C}$ -TOC) isotopic compositions were measured at UOttawa facilities (Jàn Veizer
214 Stable Isotope Laboratory) using EA-IRMS (Delta Advantage, Thermo Germany). The sample preparation method
215 was the same used for elemental analyses. $\delta^{13}\text{C}$ -TOC values are denoted as $\delta\text{‰} = 10^3 \left(\frac{R_{\text{sample}}}{R_{\text{standard}}} - 1 \right)$, where R is
216 ¹³C/¹²C and standards refer to the Vienna Pee Dee Belmnite (VPDP).



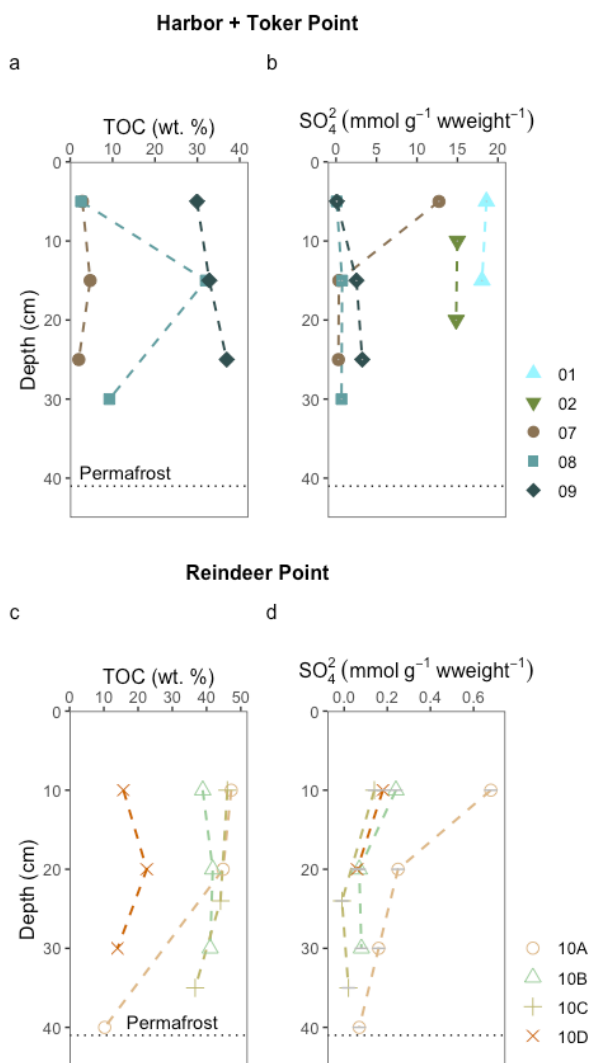
217 **2.5 Stable carbon isotopic composition of methane**

218 One incubation vial was analyzed for stable carbon isotopic composition of headspace methane ($\delta^{13}\text{C}\text{-CH}_4$).
219 Stable carbon from methane ebullition samples collected from pondlets were also analyzed. Both types of samples
220 were analyzed with a cavity ring-down spectrometer (PICARRO G2201-i isotopic CO_2/CH_4) equipped with a 16-port
221 distribution manifold and small sample introduction module (SSIM) at McGill (McGill Isotope Biogeochemistry
222 Laboratory). Incubations were kept at 4°C in the dark for 8 months to let the microbial community stabilize and
223 produce sufficient CH_4 for analysis. To stay in the detection range of the analyzer (1.8-1000 ppm CH_4), a small volume
224 of the headspace, proportional to CH_4 concentration in sample, was drawn from the incubation vial (0.2-6 mL). The
225 sample was introduced to the 16-port manifold with a 21G needle connected to a disposable luer lock plastic syringe.
226 Samples were diluted with zero air by the SSIM to reach a volume of 20 mL. Two or three measurements per sample
227 were conducted depending on headspace concentration. Ebullition gases samples were analyzed following the same
228 method. Measured values were corrected with internal certified methane standards (-59‰ and -42‰) from AirLiquide
229 and stability of the analyzer was tested with injections of ambient air. Measured values were more precise than \pm
230 1.2‰. All $\delta^{13}\text{C}\text{-CH}_4$ values are expressed relatively to VPDB.

231 **3 Results**

232 **3.1 Soil description and composition**

233 TOC content in the sampled soils ranged from 2 to 47 wt. %, with no clear trend in relation to depth (Fig 3,
234 a, c). The RP polygonal patterned ground featured organic soils with TOC content ranging from 14 to 47 wt. % (Fig
235 3, c). The TP coastal polygonal patterned ground also featured organic soils with TOC content ranging from 2 to 37
236 wt. % (Fig 3, a).



237

238 **Figure 3.** Total organic carbon and sulfate (SO_4^{2-}) concentrations in sediment or soil from the active layer of different
 239 sites in this study. The datasets are separated into two for clarity. The upper part of the figure (panels A and B) displays
 240 the data of the marine site Harbor (profile 01 and 02), and the coastal site, Toker Point (profile 07, 08 and 09). The
 241 lower part of the figure (panel C and D) displays the data from the inland site Reindeer Point (profile 10A, 10B, 10C
 242 and 10D). The black horizontal dotted line in each graph represents the permafrost-active layer interface except for
 243 the Harbor site, where the active layer is much deeper but not measured. TOC data from Harbor site is not available.
 244 A uniform color pattern is used throughout this article.

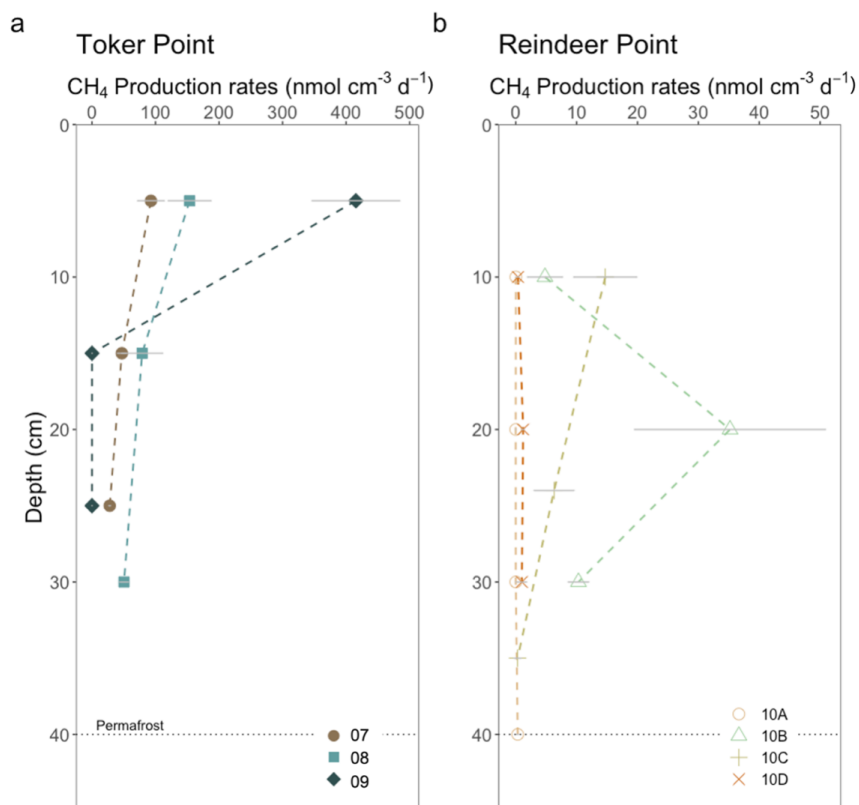
245 RP, the inland site, had low sulfate and chloride concentrations relative to TP, the coastal site (Fig 3 (b), (d)
 246 and S2). Sulfates at RP ranged from null concentrations to $0,68 \pm 0.03 \text{ mmol g}^{-1} \text{ wweight}^{-1}$, while at TP, profiles



247 exhibited varying concentrations and patterns in relation to depth. Sulfate concentrations, ranged from 0.07 ± 0.03 to
248 $12.72 \pm 0.03 \text{ mmol g}^{-1} \text{ wweight}^{-1}$. Profile 07, the low-centered polygon, exhibited the highest sulfates concentrations
249 of all TP site at its surface ($12.72 \pm 0.03 \text{ mmol g}^{-1} \text{ wweight}^{-1}$), with concentrations decreasing drastically with depth,
250 reaching $0.29 \pm 0.03 \text{ mmol g}^{-1} \text{ wweight}^{-1}$ at 25 cm (Fig 3, a). In profile 09, the high-centered polygon, sulfate
251 concentrations increased with depth ranging from $0.09 \pm 0.03 \text{ mmol g}^{-1} \text{ wweight}^{-1}$ at 5 cm to $3.2 \pm 0.03 \text{ mmol g}^{-1}$
252 wweight^{-1} at 25 cm. Finally, profile 08, characterized as a polygonal trough, had sulfate concentrations ranging from
253 0.07 ± 0.03 to $0.75 \pm 0.03 \text{ mmol g}^{-1} \text{ wweight}^{-1}$. The highest sulfate concentrations measured in this study were found
254 in the sediments of the Harbor site, with a mean value of $16.6 \text{ mmol g}^{-1} \text{ wweight}^{-1}$ (Fig 3, a).

255 3.2 Methane production

256 Rates of CH_4 production in incubations of sediment and soil with brackish water were undertaken at the three
257 studied sites: RP, TP and Harbor. Production rates ranged from null to $415.4 \pm 69.2 \text{ nmol cm}^{-3} \text{ d}^{-1}$ (Fig 4) throughout
258 all samples in this study. At RP, the maximum CH_4 production rate of $35.2 \pm 15.7 \text{ nmol cm}^{-3} \text{ d}^{-1}$ was measured in the
259 trough profile (10B) at a depth of 20 cm. Lower values were obtained for the surface and at the active layer-permafrost
260 interface. The low-centered polygon (10C) had its maximum CH_4 production rate in the surface, decreasing with
261 depth. High-centered polygons (10A and 10D) had very low production rates along their depth profiles ranging
262 between null to $1.2 \pm 0.2 \text{ nmol cm}^{-3} \text{ d}^{-1}$. Both water-saturated trough and low-centered polygon (10B,10C) had
263 relatively high CH_4 production rate compared with the high-centered polygon profiles (10A, 10D), which were water-
264 unsaturated.



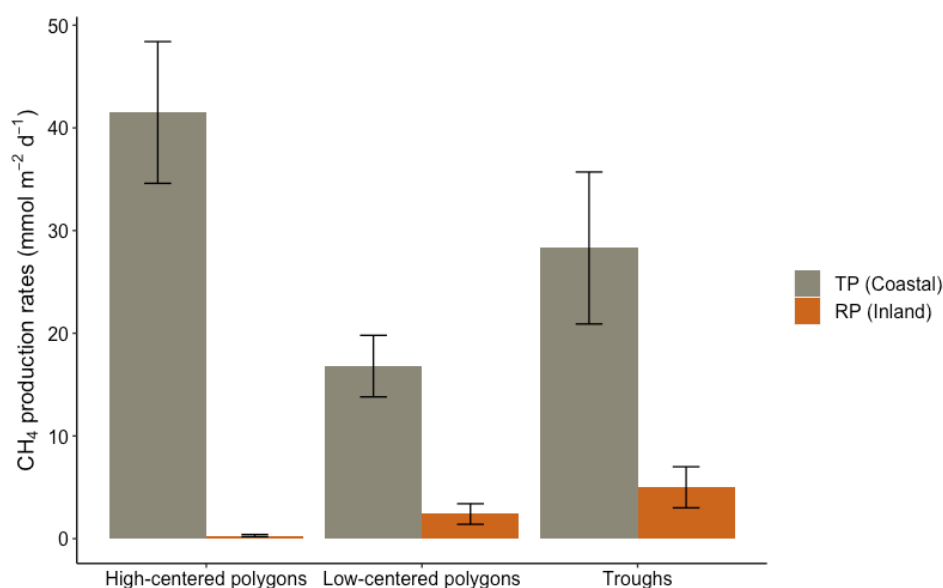
265

266 **Figure 4.** CH₄ production in incubations of soil and sediment with brackish water from (a) TP and (b) RP. Each
 267 datapoint represent the mean value of three incubations. The error bars equal to the standard deviation of the three
 268 separate incubations. Each profile corresponds to a specific landform. At Toker Point (panel A), profile 07 is from a
 269 low-centered polygon, profile 08 is from a trough and profile 09 is from a high-centered polygon. At Reindeer point
 270 (panel B), profile 10A is from a high-centered polygon, profile 10B is from a trough, profile 10C is from a low-
 271 centered polygon and profile 10D is from a high-centered polygon.

272 At TP, a maximum CH₄ production rate was recorded in profile 09, the high-centered polygon at $415.4 \pm$
 273 $69.2 \text{ nmol cm}^{-3} \text{ d}^{-1}$ at the uppermost depth but it quickly decreased in the subsurface. Profile 08, the trough, and profile
 274 07, the low-centered polygon, had lower sub-surface CH₄ production rates, but rates decreased less drastically with
 275 depth with values being relatively high at the permafrost-active layer interface. Profile 07 had values ranging from
 276 $27.9 \pm 1.5 \text{ nmol cm}^{-3} \text{ d}^{-1}$ to $92.8 \pm 21.2 \text{ nmol cm}^{-3} \text{ d}^{-1}$ and profile 08 had values ranging from $50.4 \pm 7.2 \text{ nmol cm}^{-3} \text{ d}^{-1}$
 277 and $153.7 \pm 33.9 \text{ nmol cm}^{-3} \text{ d}^{-1}$ (Fig 4). In general, at TP, the coastal site, much higher CH₄ production rates were
 278 measured than at RP, the inland site (Fig 4). The mean CH₄ production rate measured in the active layer of RP was
 279 $5.7 \text{ nmol cm}^{-3} \text{ d}^{-1}$, while at TP it was $96.2 \text{ nmol cm}^{-3} \text{ d}^{-1}$. The incubations with silty-clay Harbor sediments did not
 280 have measurable CH₄ production rates (Fig S5).



281 Estimated total active layer CH₄ production rates were calculated for each geomorphological landforms of
282 RP and TP sites. At RP, the total CH₄ production estimated for the high-centered polygons (profile 10A and 10D),
283 low-centered polygon (profile 10C) and trough (profile 10B) were $0.3 \pm 0.1 \text{ mmol m}^{-2} \text{ d}^{-1}$, $2.4 \pm 1.0 \text{ mmol m}^{-2} \text{ d}^{-1}$ and
284 $5 \pm 2 \text{ mmol m}^{-2} \text{ d}^{-1}$, respectively (Fig 5). At TP, the total CH₄ production estimated for the high-centered polygon
285 (profile 09), the low-centered polygon (profile 07) and the through (profile 08) were $41.5 \pm 6.9 \text{ mmol m}^{-2} \text{ d}^{-1}$, 16.8
286 $\pm 3.0 \text{ mmol m}^{-2} \text{ d}^{-1}$ and $28.3 \pm 7.4 \text{ mmol m}^{-2} \text{ d}^{-1}$, respectively (Fig 5). In all landforms, the active layer CH₄ production
287 rates were higher in the coastal site, TP, than the inland site, RP.

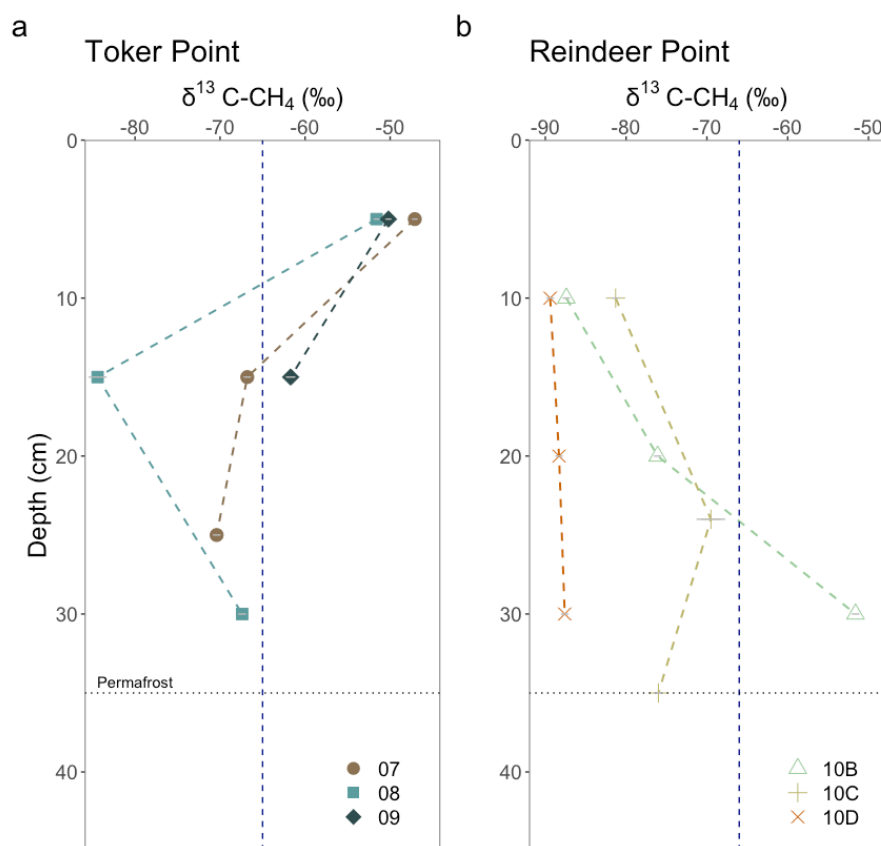


288

289 **Figure 5.** Total active layer production rates (T) at Toker Point (Coastal) and Reindeer Point (Inland) organized by
290 geomorphological forms of high-centered polygons, low-centered polygons and troughs. High-centered polygons at
291 RP is the mean of two profiles. All other landforms at RP and TP are one profile. The uncertainty on total active layer
292 production rate is propagated from the uncertainty of individual CH₄ production rates, not averages from replicate
293 sites.

294 3.3 Isotopic composition of ¹³C-CH₄

295 In parallel with CH₄ production rates, one incubation vial per depth was used to measure the stable carbon
296 isotopic composition of the CH₄ produced. At RP, the δ¹³C-CH₄ of the first sampled depth (10 cm) ranged from -
297 81.3‰ to -89.4‰. At TP, the coastal site, the δ¹³C-CH₄ signature of the first sampled depth (5 cm) ranged from -
298 47.1‰ and -51.6‰. The values cluster together based on site, suggesting surface OM degradation processes are most
299 similar within sites than between sites (Fig. 6). Profiles at RP became progressively enriched in ¹³C with depth, except
300 for profile 10C where a more depleted value was observed at 35 cm. Conversely, at TP, profiles became depleted in
301 ¹³C with depth, except for profile 08 where an enrichment was measured between 15 and 30 cm.



302

303 **Figure 6.** Isotopic composition of CH_4 produced in brackish water incubations from (a) TP and (b) RP. Each datapoint
 304 corresponds to the mean value of two or three measurements done on one incubation, depending on the headspace
 305 concentration. The dashed vertical lines correspond to in situ ebullition CH_4 collected in pondlets at each sampling
 306 site ($n=1$). These values give information on the pathways used by the soil microbes to produce CH_4 . $\delta^{13}\text{C}$ between -
 307 65‰ and -50‰ is typically associated with acetoclastic methanogenesis, while $\delta^{13}\text{C}$ between -110‰ and -60‰ is
 308 associated with hydrogenotrophic methanogenesis (Hornibrook et al., 1997, 2000). The error bars on each point
 309 represents the analytical uncertainty on the measured value, otherwise the uncertainty is smaller than the point.

310 Ebullition samples from pondlets were also measured for stable isotopes. The ebullition samples represent
 311 the net $\delta^{13}\text{C}$ signature of methane produced in the sediments of pondlets at RP and TP. At RP, CH_4 ebullition from a
 312 sampled thaw pond had a $\delta^{13}\text{C}$ of -66.1‰ (fig 6). At TP, CH_4 ebullition from a sampled pondlet had a $\delta^{13}\text{C-CH}_4$ of -
 313 65.0‰ (fig 6).



314 4 Discussion

315 4.1 Addition of brackish water to anoxic incubations did not strongly suppress methanogenesis

316 Despite the addition of brackish water containing sulfate to incubations, the range of CH₄ production rates
317 measured in this study is consistent with reports for anaerobic incubations of recently thawed permafrost soils,
318 suggesting that the input of brackish water to some coastal systems may not inhibit CH₄ production. For example, in
319 the talik of Big Trail Lake, a young thermokarst lake in the interior of Alaska, CH₄ production rates based on
320 incubations ranged between 4.7 and 16.1 nmol cm⁻³ d⁻¹ (Pellerin et al., 2022), while in incubations from Vault Lake,
321 another thermokarst lake in the interior of Alaska, CH₄ production rates varied between 11.1 and 275 nmol cm⁻³ d⁻¹
322 (Heslop et al., 2015). In active layer incubations from the Yamal Peninsula in NW Siberia (Russia), CH₄ production
323 rates of incubations varied between 0.1 and 33.8 nmol cm⁻³ d⁻¹ (Heyer et al., 2002). This indicates that overall, the
324 CH₄ production rates measured at both TP and RP are within the range observed in typical ice-rich permafrost settings
325 and reasonable for the environment studied (Fig. 4). Control incubations without the addition of brackish water were
326 not included in this study. However, Lapham et al. (2021) conducted sediment incubation experiments using a core
327 collected from the coast of the Tuktoyaktuk Peninsula. In their study, CH₄ production was measured under anaerobic
328 conditions at 15 °C, without the addition of water, over a 35-day period. The reported CH₄ production rate was
329 0.07 nmol cm⁻³ d⁻¹. Although their incubations were performed over a shorter duration and at a significantly higher
330 temperature than those in the present study, the measured rate reflects CH₄ production under relatively natural,
331 unamended conditions. This value is comparable to the lowest CH₄ production rates measured in our incubations at
332 both the coastal (TP) and inland (RP) sites and provides a useful reference for CH₄ production under unamended
333 conditions.

334 The novel aspect of this study is that it attempts to understand marine influences on OM degradation by addition
335 of brackish water in anoxic active layer sediment and soil incubations between a marine site (Harbor), one that is
336 periodically submerged (TP) and never submerged (RP). This simulates the input of seawater to the active layer of
337 tundra soils (RP) as well as providing reference sites with a high marine influence (Harbor and TP). We hypothesized
338 that the addition of locally obtained brackish water, which contained sulfate (5.7 mmol L⁻¹), to the incubations, would
339 suppress CH₄ production in RP, the inland site and potentially also at TP, the coastal site. This reasoning is because
340 supplying sulfate to low sulfate organic-rich sediment would promote sulfate reduction, which is thermodynamically
341 more favorable than methanogenesis, thereby competitively inhibiting it (Lovely and Klug, 1983; Oremland and
342 Polcin, 1982). This hypothesis is also consistent with field observations; organic matter mineralization in brackish
343 wetlands is consistently dominated by bacterial sulfate reduction (Bridgman et al., 2013; Torres-Alvarado et al., 2005)
344 where little to no CH₄ emissions are observed (Pönisch et al., 2022; Petersen et al., 2023; Kroeger et al., 2017).

345 RP had low sulfate concentrations before addition of the brackish water but so did many of the profiles from TP
346 (Fig 3). In the Harbor sediments, no methane production was observed (Fig S5). This is consistent with the competitive
347 inhibition of methanogenesis by energetically favorable redox reactions with electron acceptors like oxygen, nitrate,
348 iron oxides or sulfate that is typical of marine systems e.g. (Martens and Berner, 1974) as well as the potential for
349 anaerobic oxidation of methane (AOM). Given that the Harbor sediments already had high sulfate concentrations, the



350 lack of methane production with addition of brackish water was expected. However, strong CH₄ production was
351 observed in the incubations of both the coastal site TP and the inland site RP, indicating that CH₄ production was not
352 halted by the addition of sulfate via the brackish water addition at those sites. While sulfate reduction rates were not
353 measured, a strong sulfide smell was recorded when opening most of the incubations at the end of the experiment,
354 likely indicating the coexistence of sulfate reduction and methanogenesis during the incubations.

355 Coexistence of sulfate and methanogenesis within complex sediment systems such as estuarine, coastal and salt
356 marsh sediments has been widely reported (Lovley et al., 1982; Oremland and Taylor, 1978; Sela-Adler et al., 2017).
357 Two main mechanisms are invoked to explain this co-existence in our incubation experiment: (1) noncompetitive
358 methanogenesis (i.e. methylotrophic methanogenesis) and (2) syntrophic methanogenesis. (1) Noncompetitive
359 substrates are substrates like methanol and methylamines that are used by methanogens alone and cannot be used with
360 electron acceptors like sulfate (Lovley and Klug, 1983; Oremland et al., 1982). Noncompetitive substrates are thus
361 microbially converted to CH₄, even in sediments with high sulfate concentrations (Maltby et al., 2018; Yuan et al.,
362 2019). For example, in salt marshes, where high sulfate concentrations are often found, elevated CH₄ emissions are
363 suggested to mainly stem from noncompetitive methanogenesis (Comer-Warner et al., 2022; Poffenbarger et al., 2011;
364 Yuan et al., 2019). In the sulfate reducing zone of sediments from the Baltic Sea, where ample sulfate is found in the
365 porewaters, seasonal methanogenesis rates were measured up to 1.3 nmol cm⁻³ d⁻¹ due to noncompetitive substrates
366 (Maltby et al., 2018). In permafrost soils, methanol, methylamines and the microorganisms capable of degrading them
367 have been observed but their concentrations are typically low (Coolen and Orsi, 2015; Kramshoj et al., 2018).
368 However, our study sites are on a coast undergoing a rapid transgression which may be driving imbalances between
369 substrate supply and microbial abundances. The rates of methane production observed at RP and TP of up to 154 nmol
370 cm⁻³ d⁻¹ contrast with reported values for methylotrophic methanogenesis (Maltby et al., 2018). Based on these
371 numbers, noncompetitive substrates likely play a small role in the total methane production at our study sites but
372 further investigation into methylotrophic methane production in coastal environments will allow to document the
373 overall role of methylotrophic methane production in coastal permafrost settings.

374 (2) Syntrophic methanogenesis occurs when molecular hydrogen produced by acetoclastic sulfate-reducing
375 bacteria is used by hydrogenotrophic methanogens. In this syntrophy, the chemical energy is shared via interspecies
376 hydrogen transfer (Ozuolmez et al., 2015). For instance, in permafrost soils of Sweden, it was demonstrated that
377 syntrophic methanogenesis was favored in anoxic and water-saturated soils by an elevated abundance in methanogens
378 and their syntrophic partners (Keuschnig et al., 2022). As the incubation experiment in our study at RP and TP featured
379 water-saturated and anoxic environments, syntrophic methanogenesis could participate in the co-occurrence of sulfate-
380 reduction and methanogenesis. This mechanism is consistent with most incubations producing methane with a δ¹³C
381 value in the range of hydrogenotrophic methanogenesis (see below).

382 Measuring methane production through incubations inherently has limitations as they prevent continuous inputs
383 of microorganisms, fresh OM and nutrients that would occur in the natural environment. This can create a “bottle
384 effect”, which leads to restrictions in microbial community composition, limits the input of nutrients and leads to the
385 accumulation of metabolites which would normally be degraded (Ionescu et al., 2015). Typically, overestimation of



386 microbial processes rates is observed compared to *in situ* data (Sherr et al., 1999). The overestimation of CH₄
387 production rates by incubations relative to the *in situ* rates are difficult to assess because of a lack of data in permafrost
388 environments (Heslop et al., 2020). Furthermore, a lag time between the start of anaerobic incubations and maximum
389 CH₄ production rate is widely documented, which appears to be the case for both active layer and thawed permafrost
390 incubations (Holm et al., 2020; Knoblauch et al., 2018; Knoblauch et al., 2013; Roy Chowdry et al., 2015). Drier or
391 water-unsaturated conditions lead to a longer lag time before the onset of maximum CH₄ production (Treat et al.,
392 2015). Microbial community composition in the soil or sediment also exerts a strong control on the organic carbon
393 degradation and has been shown to change throughout the incubations (Holm et al., 2020). Low initial methanogen
394 population in soils can contribute to this lag time, but other factors such as disturbance of sediment during sampling,
395 substrate availability and redox state can also contribute to the observed lag time in some incubations (Treat et al.,
396 2015; Roy Chowdry et al., 2015).

397 Furthermore, it is also possible that a “priming effect” from the addition of brackish water in incubations could
398 have supercharged OM degradation with marine organic carbon, nutrients and microorganisms (Bianchi, 2011), which
399 may have enhanced CH₄ production. However, this priming effect was not observed in the Harbor sediments which
400 were amended with the same brackish water. Furthermore, CH₄ ebullition samples collected from pondlets adjacent
401 to RP and TP exhibited broadly similar $\delta^{13}\text{C}$ values to methane produced in incubations (Fig 6), suggesting a similitude
402 in microbial degradation pathways to methane *in situ* and in the incubations. Despite these uncertainties, our dataset
403 shows clear depth trends and landscape-level variations, indicating that even under brackish water addition, local
404 conditions will strongly influence CH₄ production.

405 **4.2 CH₄ production pathways depend on hydrology and organic matter lability**

406 The addition of brackish water resulted in incubation conditions being water-saturated in all cases, but it
407 appears that biological and hydrological conditions of the polygonal patterned grounds influenced the magnitude of
408 CH₄ production, nonetheless.

409 In all landforms, the active layer CH₄ production rates were lower at the inland site, RP than at TP, the coastal
410 site (Fig 4). Inland, low-centered polygons and troughs have typically higher CH₄ fluxes than unsaturated landforms
411 like high-centered polygons (Roy Chowdry et al., 2015; Martin et al., 2018; Zheng et al., 2018) which indicates they
412 likely also have higher CH₄ production rates. Within sites in our study, brackish water amended incubations of high-
413 centered polygon soils had lower CH₄ production rates, while brackish water amended incubations of troughs and low-
414 centered polygons had higher CH₄ production rates (Fig 4). This indicates that for the degradation of organic matter
415 into CH₄ in tundra soils, increasing seawater interactions through coastal processes, such as submersion due to
416 subsidence or increased storm severity, resulting in the input of seawater in terrestrial soils, does not halt CH₄
417 production. It also shows that landforms and local hydrology remain important in controlling the microbial
418 communities which affects the resulting CH₄ production.

419 Marine OM and nutrient inputs from tides and storm surges may contribute to the higher lability of OM and
420 could fuel greater fermentation (Valdemarsen and Kristensen, 2010). It was reported that 8.7% of the organic carbon



421 in nearshore sediments of Herschel Island, Beaufort Sea, came from marine sources (Couture et al., 2018). This is
422 relevant for the TP site because while $\delta^{13}\text{C}$ signature of soils showed that terrestrial OM is dominant (Fig S4), marine
423 OM may get transported and deposited in coastal soils during high tides and storm surges. Although our analyses
424 could not detect the presence of marine OM in TP soils, the higher CH_4 production rates recorded in the incubations
425 of TP, relatively to those of RP could in part be explained by marine OM and nutrient inputs. Interestingly, the high-
426 centered polygon at TP, profile 09 (Fig 4), did not behave in a predictable manner, since it had very high CH_4
427 production rates on the surface. This may be due to the presence of high levels of geese fecal matter on the surface at
428 TP, profile 09, which may provide a significant source of labile organic carbon or nutrients like N and P and a different
429 microbial community composition on surface sediments, capable of high CH_4 production rates immediately following
430 the start of the incubations. Lower in the profile, CH_4 production rates were very low, characteristic of the CH_4
431 production rates observed in water-unsaturated high-centered polygons (Fig 4). Therefore, in this instance, proximity
432 with the coast may have influenced CH_4 production through the presence of fauna.

433 Stable carbon isotopic signature of CH_4 provides insights on the microbial processes involved in
434 methanogenesis and on substrates used. $\delta^{13}\text{C}\text{-CH}_4$ between -65% and -50% is typically associated with acetoclastic
435 methanogenesis, while $\delta^{13}\text{C}\text{-CH}_4$ between -110% and -60% is associated with hydrogenotrophic methanogenesis
436 (Hornibrook et al., 1997, 2000). The stable isotopic signature of methylotrophic methanogenesis is between -83% and
437 -72% (Penger et al., 2012), which overlaps with the hydrogenotrophic interval, precluding us from separating these
438 two metabolic pathways. At RP, except for profile 10B, $\delta^{13}\text{C}\text{-CH}_4$ had more negative values, consistent with the
439 processing of recalcitrant organic matter through the hydrogenotrophic production pathway (Heffernan et al., 2022;
440 Hodgkins et al., 2014). Profile 10B, a polygonal trough, had less negative $^{13}\text{C}\text{-CH}_4$ values more consistent with
441 acetoclastic methanogenesis (Hornibrook et al., 1997). At TP, the coastal polygonal tundra, $\delta^{13}\text{C}\text{-CH}_4$ at 5 cm depth
442 is less negative, consistent with methanogenesis with more labile organic carbon and the acetoclastic production
443 pathway (Hodgkins et al., 2014), transitioning to more negative values, associated to hydrogenotrophic production
444 with depth. This shift suggests an input of labile OM in TP surface and sub-surface soils. This may be due to the labile
445 OM from abundant geese fecal matter that was observed in the surface. It is also possible that *Carex sp.*, the dominant
446 plant species of the site, may be a source of labile fermentation precursors (Galand et al., 2010; Liebner et al., 2015).

447 By comparing the CH_4 production rates from brackish water incubations from RP and TP we infer that the
448 simple addition of brackish water is not the only parameter controlling CH_4 production between inland and coastal
449 sites. Other interactions from coastal processes must enhance CH_4 production in the coastal site. Investigating the
450 potential role of additional marine organic matter inputs will be crucial to better understanding the carbon cycling in
451 Arctic coastal environments.

452 **4.3 Active layer CH_4 production rates are comparable to the net CH_4 fluxes measured in similar environments**

453 In a polygonal terrain of the Tuktoyaktuk Coastlands, net CH_4 fluxes from the center of high-centered polygons
454 and troughs derived from flux chambers were measured to be $1.9 \pm 20.4 \text{ mmol m}^{-2} \text{ d}^{-1}$ and $13.0 \pm 20.4 \text{ mmol m}^{-2} \text{ d}^{-1}$
455 respectively (Martin et al., 2018). These overlap with values of estimated total CH_4 production derived from the



456 brackish water amended incubation experiments (Fig. 5). It is clear from the large variations in measured CH₄
457 emissions from the study of Martin et al., (2018) that incubations to estimate total active layer CH₄ production rates
458 can discern small differences due to local variations that stem mostly from the polygonal features. For example, at
459 RP a comparable polygonal terrain located in the same study area of Martin et al., (2018), the active layer of high-
460 centered polygons and trough, produced $0.3 \pm 0.1 \text{ mmol m}^{-2} \text{ d}^{-1}$ and $5.0 \pm 2.0 \text{ mmol m}^{-2} \text{ d}^{-1}$ (Fig. 5), respectively which
461 are significantly different. This indicates the role of polygonal forms in controlling the activity of microbial
462 communities which controls CH₄ production and the potential to scale more accurately CH₄ production at the
463 landscape level based on landform distributions.

464 Interestingly, TP, the coastal site, had an estimated total active layer CH₄ production rate comparable to emissions
465 of a St. Lawrence estuary salt marsh which had a CH₄ flux of $24 \pm 14.4 \text{ mmol m}^{-2} \text{ d}^{-1}$ (Comer-Warner et al., 2022).
466 The St. Lawrence estuary salt marshes are affected by freeze-thaw cycles associated with seasons comparable to the
467 freeze-thaw cycles observed in the active layer of Tuktoyaktuk coastlands despite lacking some characteristics features
468 of our site like the presence of permafrost and rapid coastal erosion rates. CH₄ emissions and production within areas
469 of coastal influence thus appear of similar magnitude. By comparison, mangrove forests, which are a major global
470 source of CH₄ but a very different environment from coastal Arctic polygon terrain, had average CH₄ fluxes to the
471 atmosphere of $0.3 \pm 0.1 \text{ mmol m}^{-2} \text{ d}^{-1}$ (Rosentreter et al., 2018). In another study, the average measured CH₄ flux
472 from a Yangtze Estuary (China) tidal salt marsh, with a subtropical monsoon climate, was $2.4 \text{ mmol m}^{-2} \text{ d}^{-1}$ (Li et al.,
473 2021). These reported values are similar to our study as well as other studies in the region and adds to the notion that
474 Arctic coasts are an important source of CH₄ globally that warrant further investigation.

475 The calculated total active layer methane production rates (T) from TP and RP do not take into account aerobic
476 and anaerobic oxidation of CH₄, which will most likely reduce fluxes of CH₄ from these sites. Studies and models of
477 Arctic soils emissions have highlighted that aerobic methanotrophy could consume more than half of the CH₄
478 produced in soils, greatly limiting surface emissions (Oh et al., 2020; Zheng et al., 2018). Furthermore, AOM has been
479 shown to play an important role in attenuating CH₄ production in soils and sediments (Segarra et al., 2013; Winkel et
480 al., 2019). However, AOM did not appear to influence significantly CH₄ production in incubations with thermokarst
481 lake sediments (Lotem et al., 2023). For the discussion of this study, we compared results of brackish water incubations
482 to CH₄ emissions measured in other landscapes. Such comparisons provide valuable context by comparing long-term
483 microbial production processes with net atmospheric fluxes. However, we emphasize that CH₄ production rates cannot
484 be directly equated to CH₄ emissions.

485

486

487

488



489 **Table 1.** Total methane active layer production in a context of brackish water addition in high-centered polygons,
490 low-centered polygons and troughs during growing season applied to the spatial scale of the polygonal landscape of
491 RP. Two samples were taken for the high-centered polygon. The mean active layer depth of the region is 35 cm. The
492 error represents the propagation of the analytical uncertainty from the incubations results.

Geomorphological form	Relative area of each landform (km ²)	Estimated Total CH ₄ production in active layer (mol d ⁻¹)
High-centered polygons	0.0803	20.7 ± 10.3
Low-centered polygons	0.119	284 ± 123
Troughs	0.0362	182 ± 73.4

493

494 In order to better frame the potential impact of brackish water addition at scale, we extrapolated its consequence
495 to a 25 hectare area of polygonal tundra surrounding RP (Fig S2). This estimate simulates CH₄ production following
496 the infiltration of brackish water into the terrestrial polygonal landscape around Tuktoyaktuk. This event could result
497 from coastal flooding during storm surges, which are frequent in the Mackenzie River delta (Kokelj et al., 2012;
498 Solomon et al., 2005). Taking into consideration the distribution of the polygonal features within RP and the relative
499 areas of each landform, the CH₄ production rates in the active layer, excluding pondlets, for an area of 25 ha was
500 calculated to be 487 mol d⁻¹ (Table 1) or 22 nmol m⁻² s⁻¹ and is consistent with the CH₄ emissions measured from
501 various wetland types (Cui et al., 2024). The increasing sensitivity of wetlands to climate change and the preponderant
502 role of carbon substrate availability in controlling global methane emissions (Hu et al., 2024) warrants further
503 investigating CH₄ dynamics in thawing continuous permafrost landscapes and the role of coastal processes influencing
504 these emissions. More polygonal tundra in various settings should be investigated as a comparison to the studied
505 region. Further research on aerobic and anaerobic CH₄ oxidation is necessary to provide a more precise estimate of
506 the CH₄ cycle inputs and outputs in a scope of the evaluation of its impacts on the greenhouse gas feedback loop.

507 5 Conclusions

508 The primary hypothesis for this study was that an increase in waterlogged environments due to coastal
509 flooding and inundation processes would not enhance CH₄ production because of sulfate present in coastal waters.
510 However, our incubation experiments revealed high CH₄ production rates in the presence of sulfates. Additionally,
511 waterlogged conditions attributed to the ebb and flow of tides, seems to favor anoxic OM degradation and may
512 potentially provide inputs of fresh OM and nutrients from marine sources, contributing to the elevated CH₄ production
513 rates measured in the coastal setting of TP. Moreover, no conclusive explanation for the co-occurrence of sulfate-
514 reduction and methanogenesis in our brackish water incubations was identified, but based on evidence, we suggest
515 syntrophic methanogenesis could support this co-occurrence. More investigation on methylotrophic methanogenesis
516 in coastal soils are needed as it can be an important process in saline environments (Conrad, 2020). Future studies



517 should investigate CH₄ oxidation processes in greater detail, as they could provide crucial insights into Arctic coastal
518 carbon cycling in sediments and soils affected by changing sea level.

519 **Data availability**

520 All raw data of incubation experiment and other analyses performed and generated by study are available as
521 supplementary information.

522 **Competing interests**

523 The authors declare that they have no conflict of interest.

524 **Author contributions**

525 AP designed the experiment; ARL executed the experiments and analyses. AP, ARL, DW, RL participated in the
526 fieldwork. PMJD provided lab space, equipment and insights for the stable carbon isotopes analyses on incubation
527 CH₄. RL performed all GIS analyses and maps. ARL performed the data interpretation and generated all figures. AP
528 provided expertise on the writing and interpretation of figures. All authors reviewed and edited the manuscript.

529 **Acknowledgements**

530 We thank Santiago Mareque for assistance during field sampling. Mathieu Babin and Thi Hao Bui are acknowledged
531 for assisting with the laboratory work performed at Université du Québec à Rimouski and at McGill University,
532 respectively. Tukuyvik Laboratory is acknowledged for providing analyses and results on δ¹³C and TOC content of
533 sediments. We also thank the community of Tuktoyaktuk for providing wildlife monitors with insightful information
534 on the territory during field sampling. This research was funded by NSERC Discovery Grant and Northern Supplement
535 to AP. ARL acknowledges financial support from the NSERC Northern Scientific Training Program. PMJD
536 acknowledges support from the NSERC Discovery Grant and the Canadian Foundation for Innovation.

537 **Financial support**

538 Support funds and grant agreement numbers are listed as specified upon manuscript registration.

539 **References**

- 540 AMAP, 2019. AMAP Climate Change Update 2019: An Update to Key Findings of Snow, Water, Ice and Permafrost
541 in the Arctic (SWIPA) 2017. Arctic Monitoring and Assessment Programme (AMAP), Oslo, Norway. 12 pp.
- 542 AMAP, 2017. Snow, Water, Ice and Permafrost in the Arctic (SWIPA) 2017. Arctic Monitoring and Assessment
543 Programme (AMAP), Oslo, Norway. xiv + 269 pp
- 544 Andrachuk, M., & Smit, B. (2012). Community-based vulnerability assessment of Tuktoyaktuk, NWT, Canada to
545 environmental and socio-economic changes. *Regional Environmental Change*, 12(4), 867–885.
546 <https://doi.org/10.1007/s10113-012-0299-0>



- 547 Bianchi, T. S. (2011). The role of terrestrially derived organic carbon in the coastal ocean: A changing paradigm and
548 the priming effect. *Proceedings of the National Academy of Sciences*, 108(49), 19473–19481.
549 <https://doi.org/10.1073/pnas.1017982108>
- 550 Boetius, A., Ravensschlag, K., Schubert, C. J., Rickert, D., Widdel, F., Gieseke, A., Amann, R., Jørgensen, B. B.,
551 Witte, U., & Pfannkuche, O. (2000). A marine microbial consortium apparently mediating anaerobic oxidation
552 of methane. *Nature*, 407(6804), 623–626. <https://doi.org/10.1038/35036572>
- 553 Comer-Warner, S. A., Ullah, S., Ampuero Reyes, W., Krause, S., & Chmura, G. L. (2022). *Spartina alterniflora* has
554 the highest methane emissions in a St. Lawrence estuary salt marsh. *Environmental Research: Ecology*, 1(1),
555 011003. <https://doi.org/10.1088/2752-664X/ac706a>
- 556 Conrad, R. (2020). Importance of hydrogenotrophic, acetoclastic and methylotrophic methanogenesis for methane
557 production in terrestrial, aquatic and other anoxic environments: A mini review. *Pedosphere*, 30(1), 25–39.
558 [https://doi.org/10.1016/s1002-0160\(18\)60052-9](https://doi.org/10.1016/s1002-0160(18)60052-9)
- 559 Coolen, M. J. L., & Orsi, W. D. (2015). The transcriptional response of microbial communities in thawing Alaskan
560 permafrost soils. *Frontiers in Microbiology*, 6. <https://doi.org/10.3389/fmicb.2015.00197>
- 561 Costa, 2022. Remote sensing analysis of recent coastal change and controlling factors in Tuktoyaktuk Peninsula
562 (Beaufort Sea Coast, Canada) [Masters dissertation, University of Lisbon]. Repository of Lisbon University.
563 [https://repositorio.ul.pt/>Costa Bernardo TM 2022](https://repositorio.ul.pt/>Costa%20Bernardo%20TM%202022)
- 564 Couture, N. J., Irrgang, A., Pollard, W., Lantuit, H., & Fritz, M. (2018). Coastal Erosion of Permafrost Soils Along
565 the Yukon Coastal Plain and Fluxes of Organic Carbon to the Canadian Beaufort Sea. *Journal of Geophysical*
566 *Research: Biogeosciences*, 123(2), 406–422. <https://doi.org/10.1002/2017JG004166>
- 567 Cui, S., Liu, P., Guo, H., Nielsen, C. K., Pullens, J. W. M., Chen, Q., Pugliese, L., & Wu, S. (2024). Wetland
568 hydrological dynamics and methane emissions. *Communications Earth & Environment*, 5(1).
569 <https://doi.org/10.1038/s43247-024-01635-w>
- 570 Bridgman, S. D., Cadillo-Quiroz, H., Keller, J. K., & Zhuang, Q. (2012). Methane emissions from wetlands:
571 biogeochemical, microbial, and modeling perspectives from local to global scales. *Global Change Biology*,
572 19(5), 1325–1346. <https://doi.org/10.1111/gcb.12131>
- 573 Dallimore, S. R., Wolfe, S. A., Matthews Jr., J. V., & Vincent, J.-S. (1997). Mid-Wisconsinan eolian deposits of the
574 Kittigazuit Formation, Tuktoyaktuk Coastlands, Northwest Territories, Canada. *Canadian Journal of Earth*
575 *Sciences*, 34(11), 1421–1441. <https://doi.org/10.1139/e17-116>
- 576 Elberling, B., Michelsen, A., Schädel, C., Schuur, E. A. G., Christiansen, H. H., Berg, L., Tamstorf, M. P., &
577 Sigsgaard, C. (2013). Long-term CO₂ production following permafrost thaw. *Nature Climate Change*, 3(10),
578 890–894. <https://doi.org/10.1038/nclimate1955>
- 579 Froelich, P., Klinkhammer, G., Bender, M., Luedtke, N., Heath, G., Cullen, D., Dauphin, P., Hammond, D., Hartman,
580 B., & Maynard, V. (1979). Early oxidation of organic matter in pelagic sediments of the eastern equatorial
581 Atlantic: suboxic diagenesis. *Geochimica Et Cosmochimica Acta*, 43(7), 1075–
582 1090. [https://doi.org/10.1016/0016-7037\(79\)90095-4](https://doi.org/10.1016/0016-7037(79)90095-4)
- 583 Fu, Q. A., Boutton, T. W., Ehleringer, J. R., & Flagler, R. B. (1993). Environmental and Developmental Effects on
584 Carbon Isotope Discrimination by Two Species of *Phaseolus*. In *Stable Isotopes and Plant Carbon-water*
585 *Relations* (pp. 297–309). Elsevier. <https://doi.org/10.1016/B978-0-08-091801-3.50028-3>



- 586 Galand, P. E., Yrjälä, K., & Conrad, R. (2010). Stable carbon isotope fractionation during methanogenesis in three
587 boreal peatland ecosystems. *Biogeosciences*, 7(11), 3893–3900. <https://doi.org/10.5194/bg-7-3893-2010>
- 588 Guimond, J. A., Mohammed, A. A., Walvoord, M. A., Bense, V. F., & Kurylyk, B. L. (2021). Saltwater Intrusion
589 Intensifies Coastal Permafrost Thaw. *Geophysical Research Letters*, 48(19), e2021GL094776.
590 <https://doi.org/10.1029/2021GL094776>
- 591 Heffernan, L., Cavaco, M. A., Bhatia, M. P., Estop-Aragónés, C., Knorr, K.-H., & Olefeldt, D. (2022). High peatland
592 methane emissions following permafrost thaw: Enhanced acetoclastic methanogenesis during early successional
593 stages. *Biogeosciences*, 19(12), 3051–3071. <https://doi.org/10.5194/bg-19-3051-2022>
- 594 Heslop, J. K., Walter Anthony, K. M., Sepulveda-Jauregui, A., Martinez-Cruz, K., Bondurant, A., Grosse, G., & Jones,
595 M. C. (2015). Thermokarst lake methanogenesis along a complete talik profile. *Biogeosciences*, 12(14), 4317–
596 4331. <https://doi.org/10.5194/bg-12-4317-2015>
- 597 Heslop, J. K., Walter Anthony, K. M., Winkel, M., Sepulveda-Jauregui, A., Martinez-Cruz, K., Bondurant, A., Grosse,
598 G., & Liebner, S. (2020). A synthesis of methane dynamics in thermokarst lake environments. *Earth-Science*
599 *Reviews*, 210, 103365. <https://doi.org/10.1016/j.earscirev.2020.103365>
- 600 Heyer, J., Berger, U., Kuzin, I. L., & Yakovlev, O. N. (2002). Methane emissions from different ecosystem structures
601 of the subarctic tundra in Western Siberia during midsummer and during the thawing period. *Tellus B*, 54(3),
602 231–249. <https://doi.org/10.1034/j.1600-0889.2002.01280.x>
- 603 Hill, P. R., Héquette, A., & Ruz, M.-H. (1993). Holocene sea-level history of the Canadian Beaufort shelf. *Canadian*
604 *Journal of Earth Sciences*, 30(1), 103–108. <https://doi.org/10.1139/e93-009>
- 605 Hodgkins, S. B., Tfaily, M. M., McCalley, C. K., Logan, T. A., Crill, P. M., Saleska, S. R., Rich, V. I., & Chanton, J.
606 P. (2014). Changes in peat chemistry associated with permafrost thaw increase greenhouse gas production.
607 *Proceedings of the National Academy of Sciences*, 111(16), 5819–5824.
608 <https://doi.org/10.1073/pnas.1314641111>
- 609 Holm, S., Walz, J., Horn, F., Yang, S., Grigoriev, M. N., Wagner, D., Knoblauch, C., & Liebner, S. (2020).
610 Methanogenic response to long-term permafrost thaw is determined by paleoenvironment. *FEMS Microbiology*
611 *Ecology*, 96(3), fiae021. <https://doi.org/10.1093/femsec/fiae021>
- 612 Hornibrook, E. R. C., Longstaffe, F. J., & Fyfe, W. S. (2000). Evolution of stable carbon isotope compositions for
613 methane and carbon dioxide in freshwater wetlands and other anaerobic environments. *Geochimica et*
614 *Cosmochimica Acta*, 64(6), 1013–1027. [https://doi.org/10.1016/S0016-7037\(99\)00321-X](https://doi.org/10.1016/S0016-7037(99)00321-X)
- 615 Hornibrook, E. R., Longstaffe, F. J., & Fyfe, W. S. (1997). Spatial distribution of microbial methane production
616 pathways in temperate zone wetland soils: Stable carbon and hydrogen isotope evidence. *Geochimica Et*
617 *Cosmochimica Acta*, 61(4), 745–753. [https://doi.org/10.1016/s0016-7037\(96\)00368-7](https://doi.org/10.1016/s0016-7037(96)00368-7)
- 618 Hu, H., Chen, J., Zhou, F., Nie, M., Hou, D., Liu, H., Delgado-Baquerizo, M., Ni, H., Huang, W., Zhou, J., Song, X.,
619 Cao, X., Sun, B., Zhang, J., Crowther, T. W., & Liang, Y. (2024). Relative increases in CH₄ and CO₂ emissions
620 from wetlands under global warming dependent on soil carbon substrates. *Nature Geoscience*, 17(1), 26–31.
621 <https://doi.org/10.1038/s41561-023-01345-6>
- 622 Hu, K., Issler, D., Chen, Z., & Brent, T. (2013). *Permafrost investigation by well logs, and seismic velocity and*
623 *repeated shallow temperature surveys, Beaufort-Mackenzie Basin*. <https://doi.org/10.4095/293120>



- 624 Hynes, S., Solomon, S. M., & Whalen, D. (2014). *GIS compilation of coastline variability spanning 60 years in the*
625 *Mackenzie Delta and Tuktoyaktuk in the Beaufort Sea* (7685; p. 7685). <https://doi.org/10.4095/295579>
- 626 Ionescu, D., Bizic-Ionescu, M., Khalili, A., Malekmohammadi, R., Morad, M. R., de Beer, D., & Grossart, H.-P.
627 (2015). A new tool for long-term studies of POM-bacteria interactions: Overcoming the century-old Bottle
628 Effect. *Scientific Reports*, 5(1), 14706. <https://doi.org/10.1038/srep14706>
- 629 Irrgang, A. M., Bendixen, M., Farquharson, L. M., Baranskaya, A. V., Erikson, L. H., Gibbs, A. E., Ogorodov, S. A.,
630 Overduin, P. P., Lantuit, H., Grigoriev, M. N., & Jones, B. M. (2022). Drivers, dynamics and impacts of
631 changing Arctic coasts. *Nature Reviews Earth & Environment*, 3(1), 39–54. [https://doi.org/10.1038/s43017-](https://doi.org/10.1038/s43017-021-00232-1)
632 [021-00232-1](https://doi.org/10.1038/s43017-021-00232-1)
- 633 Jones, E. L., Hodson, A. J., Thornton, S. F., Redeker, K. R., Rogers, J., Wynn, P. M., Dixon, T. J., Bottrell, S. H., &
634 O'Neill, H. B. (2020). Biogeochemical Processes in the Active Layer and Permafrost of a High Arctic Fjord
635 Valley. *Frontiers in Earth Science*, 8. <https://www.frontiersin.org/articles/10.3389/feart.2020.00342>
- 636 Keuschnig, C., Larose, C., Rudner, M., Pesqueda, A., Doleac, S., Elberling, B., Björk, R. G., Klemetsson, L., &
637 Björkman, M. P. (2022). Reduced methane emissions in former permafrost soils driven by vegetation and
638 microbial changes following drainage. *Global Change Biology*, 28(10), 3411–3425.
639 <https://doi.org/10.1111/gcb.16137>
- 640 Knoblauch, C., Beer, C., Liebner, S., Grigoriev, M. N., & Pfeiffer, E.-M. (2018). Methane production as key to the
641 greenhouse gas budget of thawing permafrost. *Nature Climate Change*, 8(4), 309–312.
642 <https://doi.org/10.1038/s41558-018-0095-z>
- 643 Knoblauch, C., Beer, C., Sosnin, A., Wagner, D., & Pfeiffer, E.-M. (2013). Predicting long-term carbon mineralization
644 and trace gas production from thawing permafrost of Northeast Siberia. *Global Change Biology*, 19(4), 1160–
645 1172. <https://doi.org/10.1111/gcb.12116>
- 646 Kokelj, S. V., Lantz, T. C., Solomon, S., Pisaric, M. F., Keith, D., Morse, P., Thienpont, J. R., Smol, J. P., & Esagok,
647 D. (2012). Using multiple sources of knowledge to investigate northern environmental change: Regional
648 ecological impacts of a storm surge in the Outer Mackenzie Delta, N.W.T. *ARCTIC*, 65(3).
649 <https://doi.org/10.14430/arctic4214>
- 650 Kramshøj, M., Albers, C. N., Holst, T., Holzinger, R., Elberling, B., & Rinnan, R. (2018). Biogenic volatile release
651 from permafrost thaw is determined by the soil microbial sink. *Nature Communications*, 9(1), 3412.
652 <https://doi.org/10.1038/s41467-018-05824-y>
- 653 Kroeger, K. D., Crooks, S., Moseman-Valtierra, S., & Tang, J. (2017). Restoring tides to reduce methane emissions
654 in impounded wetlands: A new and potent Blue Carbon climate change intervention. *Scientific Reports*, 7(1).
655 <https://doi.org/10.1038/s41598-017-12138-4>
- 656 La, W., Han, X., Liu, C.-Q., Ding, H., Liu, M., Sun, F., Li, S., & Lang, Y. (2022). Sulfate concentrations affect sulfate
657 reduction pathways and methane consumption in coastal wetlands. *Water Research*, 217, 118441.
658 <https://doi.org/10.1016/j.watres.2022.118441>
- 659 Lacelle, D., Fontaine, M., Pellerin, A., Kokelj, S. V., & Clark, I. D. (2019). Legacy of Holocene Landscape Changes
660 on Soil Biogeochemistry: A perspective from Paleo-Active Layers in Northwestern Canada. *Journal of*
661 *Geophysical Research Biogeosciences*, 124(9), 2662–2679. <https://doi.org/10.1029/2018jg004916>
- 662 Lantuit, H., Overduin, P. P., Couture, N., Wetterich, S., Aré, F., Atkinson, D., Brown, J., Cherkashov, G., Drozdov,
663 D., Forbes, D. L., Graves-Gaylord, A., Grigoriev, M., Hubberten, H.-W., Jordan, J., Jorgenson, T., Ødegård, R.



- 664 S., Ogorodov, S., Pollard, W. H., Rachold, V., ... Vasiliev, A. (2012). The Arctic Coastal Dynamics Database:
665 A New Classification Scheme and Statistics on Arctic Permafrost Coastlines. *Estuaries and Coasts*, 35(2), 383–
666 400. <https://doi.org/10.1007/s12237-010-9362-6>
- 667 Lapham, L. L., Dallimore, S. R., Magen, C., Henderson, L. C., Powers, L. C., Gonsior, M., Clark, B., Côté, M., Fraser,
668 P., & Orcutt, B. N. (2020). Microbial Greenhouse Gas Dynamics Associated With Warming Coastal Permafrost,
669 Western Canadian Arctic. *Frontiers in Earth Science*, 8.
670 <https://www.frontiersin.org/articles/10.3389/feart.2020.582103>
- 671 Li, Y., Wang, D., Chen, Z., Chen, J., Hu, H., & Wang, R. (2021). Methane Emissions during the Tide Cycle of a
672 Yangtze Estuary Salt Marsh. *Atmosphere*, 12(2), 245. <https://doi.org/10.3390/atmos12020245>
- 673 Liebner, S., Ganzert, L., Kiss, A., Yang, S., Wagner, D., & Svenning, M. M. (2015). Shifts in methanogenic
674 community composition and methane fluxes along the degradation of discontinuous permafrost. *Frontiers in*
675 *Microbiology*, 6. <https://doi.org/10.3389/fmicb.2015.00356>
- 676 Lim, M., Whalen, D., Martin, J., Mann, P. J., Hayes, S., Fraser, P., Berry, H. B., & Ouellette, D. (2020). Massive Ice
677 Control on Permafrost Coast Erosion and Sensitivity. *Geophysical Research Letters*, 47(17), e2020GL087917.
678 <https://doi.org/10.1029/2020GL087917>
- 679 Lipson, D. A., Zona, D., Raab, T. K., Bozzolo, F., Mauritz, M., & Oechel, W. C. (2012). Water-table height and
680 microtopography control biogeochemical cycling in an Arctic coastal tundra ecosystem. *Biogeosciences*, 9(1),
681 577–591. <https://doi.org/10.5194/bg-9-577-2012>
- 682 Lotem, N., Pellerin, A., Anthony, K. W., Gafni, A., Boyko, V., & Sivan, O. (2023). Anaerobic oxidation of methane
683 does not attenuate methane emissions from thermokarst lakes. *Limnology and Oceanography*, 68(6), 1316–
684 1330. <https://doi.org/10.1002/lno.12349>
- 685 Lovley, D. R., & Klug, M. J. (1983). Sulfate reducers can outcompete methanogens at freshwater sulfate
686 concentrations. *Applied and Environmental Microbiology*, 45(1), 187–192.
687 <https://doi.org/10.1128/aem.45.1.187-192.1983>
- 688 Mackay, J. R., & Dallimore, S. R. (1992). Massive ice of the Tuktoyaktuk area, western Arctic coast, Canada.
689 *Canadian Journal of Earth Sciences*, 29(6), 1235–1249. <https://doi.org/10.1139/e92-099>
- 690 Maltby, J., Steinle, L., Löscher, C. R., Bange, H. W., Fischer, M. A., Schmidt, M., & Treude, T. (2018). Microbial
691 methanogenesis in the sulfate-reducing zone of sediments in the Eckernförde Bay, SW Baltic Sea.
692 *Biogeosciences*, 15(1), 137–157. <https://doi.org/10.5194/bg-15-137-2018>
- 693 Martens, C. S., & Berner, R. A. (1974). Methane production in the interstitial waters of Sulfate-Depleted marine
694 sediments. *Science*, 185(4157), 1167–1169. <https://doi.org/10.1126/science.185.4157.1167>
- 695 Martin, A. F., Lantz, T. C., & Humphreys, E. R. (2018). Ice wedge degradation and CO₂ and CH₄ emissions in the
696 Tuktoyaktuk Coastlands, Northwest Territories. *Arctic Science*, 4(1), 130–145. <https://doi.org/10.1139/as-2016-0011>
- 698 Manson, G. K., Couture, N. J., & James, T. S. (2019). *CanCoast 2.0: Data and indices to describe the sensitivity of*
699 *Canada's marine coasts to changing climate* (8551; p. 8551). <https://doi.org/10.4095/314669>
- 700 Murton, J. B. (1996). Thermokarst-lake-basin sediments, Tuktoyaktuk Coastlands, western arctic Canada.
701 *Sedimentology*, 43(4), 737–760. <https://doi.org/10.1111/j.1365-3091.1996.tb02023.x>



- 702 Oh, Y., Zhuang, Q., Liu, L., Welp, L. R., Lau, M. C. Y., Onstott, T. C., Medvigy, D., Bruhwiler, L., Dlugokencky, E.
703 J., Hugelius, G., D'Imperio, L., & Elberling, B. (2020). Reduced net methane emissions due to microbial
704 methane oxidation in a warmer Arctic. *Nature Climate Change*, *10*(4), 317–321. [https://doi.org/10.1038/s41558-](https://doi.org/10.1038/s41558-020-0734-z)
705 [020-0734-z](https://doi.org/10.1038/s41558-020-0734-z)
- 706 Oremland, R. S., & Polcin, S. (1982). Methanogenesis and Sulfate Reduction: Competitive and Noncompetitive
707 Substrates in Estuarine Sediments. *Applied and Environmental Microbiology*, *44*(6), 1270–1276.
708 <https://doi.org/10.1128/aem.44.6.1270-1276.1982>
- 709 Ozuolmez, D., Na, H., Lever, M. A., Kjeldsen, K. U., Jørgensen, B. B., & Plugge, C. M. (2015). Methanogenic archaea
710 and sulfate reducing bacteria co-cultured on acetate: Teamwork or coexistence? *Frontiers in Microbiology*, *6*,
711 492. <https://doi.org/10.3389/fmicb.2015.00492>
- 712 Pellerin, A., Lotem, N., Walter Anthony, K., Eliani Russak, E., Hasson, N., Roy, H., Chanton, J. P., & Sivan, O.
713 (2022). Methane production controls in a young thermokarst lake formed by abrupt permafrost thaw. *Global*
714 *Change Biology*, *28*(10), 3206–3221. <https://doi.org/10.1111/gcb.16151>
- 715 Penger, J., Conrad, R., & Blaser, M. (2012). Stable Carbon Isotope Fractionation by Methylotrophic Methanogenic
716 Archaea. *Applied and Environmental Microbiology*, *78*(21), 7596–7602. [https://doi.org/10.1128/AEM.01773-](https://doi.org/10.1128/AEM.01773-12)
717 [12](https://doi.org/10.1128/AEM.01773-12)
- 718 Petersen, S. G. G., Kristensen, E., & Quintana, C. O. (2023). Greenhouse Gas Emissions from Agricultural Land
719 Before and After Permanent Flooding with Seawater or Freshwater. *Estuaries and Coasts*, *46*(6), 1459–1474.
720 <https://doi.org/10.1007/s12237-023-01218-6>
- 721 Poffenbarger, H. J., Needelman, B. A., & Megonigal, J. P. (2011). Salinity Influence on Methane Emissions from
722 Tidal Marshes. *Wetlands*, *31*(5), 831–842. <https://doi.org/10.1007/s13157-011-0197-0>
- 723 Pönisch, D. L., Breznikar, A., Gutekunst, C. N., Jurasinski, G., Voss, M., & Rehder, G. (2023). Nutrient release and
724 flux dynamics of CO₂, CH₄, and N₂O in a coastal peatland driven by actively induced rewetting with brackish
725 water from the Baltic Sea. *Biogeosciences*, *20*(2), 295–323. <https://doi.org/10.5194/bg-20-295-2023>
- 726 Rampton, V. N. (1988). *Quaternary geology of the Tuktoyaktuk coastlands, Northwest Territories*.
727 <https://www.osti.gov/etdweb/biblio/6877609>
- 728 Rosentreter, J. A., Maher, D. T., Erler, D. V., Murray, R. H., & Eyre, B. D. (2018). Methane emissions partially offset
729 “blue carbon” burial in mangroves. *Science Advances*, *4*(6). <https://doi.org/10.1126/sciadv.aao4985>
- 730 Roy Chowdhury, T., Herndon, E. M., Phelps, T. J., Elias, D. A., Gu, B., Liang, L., Wullschleger, S. D., & Graham,
731 D. E. (2015). Stoichiometry and temperature sensitivity of methanogenesis and CO₂ production from saturated
732 polygonal tundra in Barrow, Alaska. *Global Change Biology*, *21*(2), 722–737.
733 <https://doi.org/10.1111/gcb.12762>
- 734 Schuur, E. a. G., McGuire, A. D., Schädel, C., Grosse, G., Harden, J. W., Hayes, D. J., Hugelius, G., Koven, C. D.,
735 Kuhry, P., Lawrence, D. M., Natali, S. M., Olefeldt, D., Romanovsky, V. E., Schaefer, K., Turetsky, M. R.,
736 Treat, C. C., & Vonk, J. E. (2015). Climate change and the permafrost carbon feedback. *Nature*, *520*(7546),
737 171–179. <https://doi.org/10.1038/nature14338>
- 738 Segarra, K. E., Comerford, C., Slaughter, J., & Joye, S. B. (2013). Impact of electron acceptor availability on the
739 anaerobic oxidation of methane in coastal freshwater and brackish wetland sediments. *Geochimica Et*
740 *Cosmochimica Acta*, *115*, 15–30. <https://doi.org/10.1016/j.gca.2013.03.029>



- 741 Sepulveda-Jauregui, A., Anthony, K. M. W., Martinez-Cruz, K., Martinez-Cruz, K., Greene, S., Thalasso, F., &
742 Thalasso, F. (2015). Methane and carbon dioxide emissions from 40 lakes along a north–south latitudinal
743 transect in Alaska. *Biogeosciences*, 12(11), 3197–3223. <https://doi.org/10.5194/bg-12-3197-2015>
- 744 Sela-Adler, M., Ronen, Z., Herut, B., Antler, G., Vigderovich, H., Eckert, W., & Sivan, O. (2017). Co-existence of
745 Methanogenesis and Sulfate Reduction with Common Substrates in Sulfate-Rich Estuarine Sediments. *Frontiers*
746 *in Microbiology*, 8. <https://www.frontiersin.org/articles/10.3389/fmicb.2017.00766>
- 747 Sherr, E., Sherr, B., & Sigmon, C. (1999). Activity of marine bacteria under incubated and in situ conditions. *Aquatic*
748 *Microbial Ecology*, 20, 213–223. <https://doi.org/10.3354/ame020213>
- 749 Skoog, Douglas A., West, Donald M., Holler, F. James, Crouch, Stanley R.. (2014). *Fundamentals of Analytical*
750 *Chemistry* (Ed. 9th). Singapore: Cengage Learning.
- 751 Solomon, S. M., Whalen, D., Saper, R. & Mulvie, J. (2005). Measuring the extent of storm surge flooding on the
752 Mackenzie River Delta, Northwest Territories, Canada using synthetic aperture radar. In Proceedings of the 8th
753 International Conference on Remote Sensing for Marine and Coastal Environments.
- 754 Vardy, S. R., Warner, B. G., & Aravena, R. (1997). Holocene Climate Effects on the Development of a Peatland on
755 the Tuktoyaktuk Peninsula, Northwest Territories. *Quaternary Research*, 47(1), 90–104.
756 <https://doi.org/10.1006/qres.1996.1869>
- 757 Vaughn, L. J. S., Conrad, M. E., Bill, M., & Torn, M. S. (2016). Isotopic insights into methane production, oxidation,
758 and emissions in Arctic polygon tundra. *Global Change Biology*, 22(10), 3487–3502.
759 <https://doi.org/10.1111/gcb.13281>
- 760 Steedman, A. E., Lantz, T. C., & Kokelj, S. V. (2017). Spatio-Temporal Variation in High-Centre Polygons and Ice-
761 Wedge Melt Ponds, Tuktoyaktuk Coastlands, Northwest Territories. *Permafrost and Periglacial Processes*,
762 28(1), 66–78. <https://doi.org/10.1002/ppp.1880>
- 763 Tanski, G., Bröder, L., Wagner, D., Knoblauch, C., Lantuit, H., Beer, C., Sachs, T., Fritz, M., Tesi, T., Koch, B. P.,
764 Haghypour, N., Eglinton, T. I., Strauss, J., & Vonk, J. E. (2021). Permafrost Carbon and CO₂ Pathways Differ
765 at Contrasting Coastal Erosion Sites in the Canadian Arctic. *Frontiers in Earth Science*, 9.
766 <https://www.frontiersin.org/articles/10.3389/feart.2021.630493>
- 767 Treat, C. C., Natali, S. M., Ernakovich, J., Iversen, C. M., Lupascu, M., McGuire, A. D., Norby, R. J., Roy Chowdhury,
768 T., Richter, A., Šantrůčková, H., Schädel, C., Schuur, E. A. G., Sloan, V. L., Turetsky, M. R., & Waldrop, M.
769 P. (2015). A pan-Arctic synthesis of CH₄ and CO₂ production from anoxic soil incubations. *Global Change*
770 *Biology*, 21(7), 2787–2803. <https://doi.org/10.1111/gcb.12875>
- 771 Treat, C. C., Wollheim, W. M., Varner, R. K., Grandy, A. S., Talbot, J., & Froking, S. (2014). Temperature and peat
772 type control CO₂ and CH₄ production in Alaskan permafrost peats. *Global Change Biology*, 20(8), 2674–2686.
773 <https://doi.org/10.1111/gcb.12572>
- 774 Turetsky, M. R., Treat, C. C., Waldrop, M. P., Waddington, J. M., Harden, J. W., & McGuire, A. D. (2008). Short-
775 term response of methane fluxes and methanogen activity to water table and soil warming manipulations in an
776 Alaskan peatland. *Journal of Geophysical Research: Biogeosciences*, 113(G3).
777 <https://doi.org/10.1029/2007JG000496>
- 778 Valdemarsen, T. B., & Kristensen, E. (2010). Degradation of dissolved organic monomers and short-chain fatty acids
779 in sandy marine sediment by fermentation and sulfate reduction. *Geochimica Et Cosmochimica Acta*, 74(5),
780 1593–1605. <https://doi.org/10.1016/j.gca.2009.12.009>



- 781 Whalen, D., Forbes, D. L., Kostylev, V., Lim, M., Fraser, P., Nedimović, M. R., & Stuckey, S. (2022). Mechanisms,
782 volumetric assessment, and prognosis for rapid coastal erosion of Tuktoyaktuk Island, an important natural
783 barrier for the harbour and community. *Canadian Journal of Earth Sciences*, 59(11), 945–960.
784 <https://doi.org/10.1139/cjes-2021-0101>
- 785 Winfrey, M. R., & Ward, D. M. (1983). Substrates for Sulfate Reduction and Methane Production in Intertidal
786 Sediments. *Applied and Environmental Microbiology*, 45(1), 193–199. [https://doi.org/10.1128/aem.45.1.193-
787 199.1983](https://doi.org/10.1128/aem.45.1.193-199.1983)
- 788 Winkel, M., Sepulveda-Jauregui, A., Martinez-Cruz, K., Heslop, J. K., Rijkers, R., Horn, F., Liebner, S., & Walter
789 Anthony, K. M. (2019). First evidence for cold-adapted anaerobic oxidation of methane in deep sediments of
790 thermokarst lakes. *Environmental Research Communications*, 1(2), 021002. [https://doi.org/10.1088/2515-
791 7620/ab1042](https://doi.org/10.1088/2515-7620/ab1042)
- 792 Ye, R., Keller, J. K., Jin, Q., Bohannon, B. J., & Bridgham, S. D. (2016). Peatland types influence the inhibitory effects
793 of a humic substance analog on methane production. *Geoderma*, 265, 131–140.
794 <https://doi.org/10.1016/j.geoderma.2015.11.026>
- 795 Yuan, J., Liu, D., Ji, Y., Xiang, J., Lin, Y., Wu, M., & Ding, W. (2019). *Spartina alterniflora* invasion drastically
796 increases methane production potential by shifting methanogenesis from hydrogenotrophic to methylotrophic
797 pathway in a coastal marsh. *Journal of Ecology*, 107(5), 2436–2450. <https://doi.org/10.1111/1365-2745.13164>
- 798 Zheng, J., RoyChowdhury, T., Yang, Z., Gu, B., Wullschleger, S. D., & Graham, D. E. (2018). Impacts of temperature
799 and soil characteristics on methane production and oxidation in Arctic tundra. *Biogeosciences*, 15(21), 6621–
800 6635. <https://doi.org/10.5194/bg-15-6621-2018>